PNAS

Supporting Information for

Self-assembling paclitaxel-mediated stimulation of tumor-associated macrophages for postoperative treatment of glioblastoma

Feihu Wang[#,1,2,3], Qian Huang[4], Hao Su[1,2], Minjiao Sun[1,2,3], Zeyu Wang[1], Ziqi Chen[1,2], Mengzhen Zheng[1,2], Rami W. Chakroun[1,2], Maya K. Monroe[1,2], Daiqing Chen[3], Zongyuan Wang[1,2], Noah Gorelick[5], Riccardo Serra[5], Han Wang[1,2], Yun Guan[4,6], Jung Soo Suk[1,3,6], Betty Tyler[5], Henry Brem[5,7,8,9], Justin Hanes[1,3,7,8,9], Honggang Cui*[1,2,3,9,10]

[#]Current address: School of Biomedical Engineering, Shanghai Jiao Tong University, 800 Dongchuan Road, Shanghai 200240, PR China
[1]Department of Chemical and Biomolecular Engineering, Whiting School of Engineering, The Johns Hopkins University, Baltimore, Maryland 21218, United States.
[2]Institute for NanoBiotechnology (INBT), The Johns Hopkins University, Baltimore, Maryland 21218, United States.
[3]Center for Nanomedicine, Wilmer Eye Institute, School of Medicine, The Johns Hopkins University, Baltimore, Maryland 21231, United States.
[4]Department of Anesthesiology and Critical Care Medicine, School of Medicine, The Johns Hopkins University, Baltimore, Maryland, 21205, United States.
[5]Department of Neurosurgery, School of Medicine, The Johns Hopkins University, Baltimore, Maryland 21231, United States.
[6]Department of Neurological Surgery, School of Medicine, The Johns Hopkins University, Baltimore, Maryland 21231, United States.
[7]Department of Ophthalmology, School of Medicine, The Johns Hopkins University, Baltimore, Maryland 21231, United States.
[8]Department of Biomedical Engineering, School of Medicine, The Johns Hopkins University, Baltimore, Maryland 21231, United States.
[9]Department of Oncology and the Sidney Kimmel Comprehensive Cancer Center, School of Medicine, The Johns Hopkins University, Baltimore, Maryland 21231, United States.
[10]Department of Materials Science and Engineering, Whiting School of Engineering, The Johns Hopkins University, Baltimore, Maryland 21218, United States.
Honggang Cui
Email: hcui6@jhu.edu

This PDF file includes:

Supporting text
Figures S1 to S20
SI References

Supporting Information Text

Molecular self-assembly. PTX-iRGD conjugate was directly dissolved in deionized water at a 3 mM concentration at room temperature. The solutions were aged for at least 24 h before use in any further studies. Nanostructure morphology was then characterized using a FEI Tecnai 12 TWIN transmission electron microscope (TEM).

Rheological Analysis. Rheological experiments were carried out on a horizontal rheometer (AR1500, TA Instruments, USA) with a controlled hydrated atmosphere at 37°C. Real time gelation was assessed by loading 100 µL of PF solution between the plates. A time sweep with constant strain of 1% was conducted at a frequency of 10 Hz. At 180 s, ~10 µL of 10X PBS solution was injected into the PF solution using a 31G insulin syringe. The gel formation kinetics were assessed using changes in storage modulus (G') and loss modulus (G") as a function of time.

GSH responsive PTX release. 500 µM PTX-iRGD and 20 mM glutathione (GSH) stock solutions were prepared in water and PBS (pH 7.4), respectively. Equal volumes of PTX-iRGD and GSH solutions were mixed and the mixtures were incubated at 37°C. Samples were then analyzed using RP-HPLC to detect the released PTX at predetermined time points.

Cell viability assay. 2.5×10^3 GL-261 cells were seeded in a 96-well plate for 24 h. Then, PTX or PTX-iRGD solutions were added to the wells at different PTX concentrations, with untreated cells used as a control. After 48 h incubation, cell viability was tested using a WST-1 assay and calculated using the equation Cell Viability (%) = A570sample/A570control × 100%. IC_{50} values of PTX or PTX-iRGD were analyzed using Graph Pad Prism 5.

Tumor spheroids inhibition assay. 1×10^4 GL-261 cells were seeded into agarose coated 48-well plates and incubated for 7 days to obtain tumor spheroids. Then, PTX and PTX-iRGD were added to the wells at the PTX concentration of 10 µM. At predetermined time points, the tumor spheroids were photographed and the volume of the tumor spheroids was calculated as follows: $V=(\pi\times d_{min}\times d_{max})/6$, with d_{min} and d_{max} representing the minimum and maximum diameter of the spheroid, respectively.

DC-ELISpot assay. Brain tumor-bearing mice were treated with EF, PF, aCD47/EF, and aCD47/PF for 7 days, then dendritic cells (DCs) were isolated from spleen (*1, 2*). A mouse IFN-γ ELISPOT Kit (BD) was used. Peripheral blood mononuclear cells (PBMC) from health mice were seed at 250,000 cells per well and incubated in the presence of DCs at 10^6 cells per well (*3*). Following the vendor's protocol, plates were scanned using a CTL-ImmunoSpot Plate Reader, and data were analyzed using CTL ImmunoSpot Software.

Depletion of immune cells. To deplete $CD3^+$ T cells and $CD8^+$ T cells, tumor-bearing mice were intraperitoneally injected with anti-CD3ε (clone 145-2C11, BioXCell) and anti-CD8-α (clone 2.43, BioXCell) or isotype control (RatIgG1, BioXcell) antibodies at an initial dose of 400 mg 1 d before treatment, followed by 200 mg every 3 d. Macrophages were depleted using 300 µg anti-CSF1R (clone AFS98, BioXCell) every other day. Depletion of $CD3^+$ T cells, $CD8^+$ T cells and macrophages were confirmed using flow cytometry analysis of peripheral blood mononuclear cells.

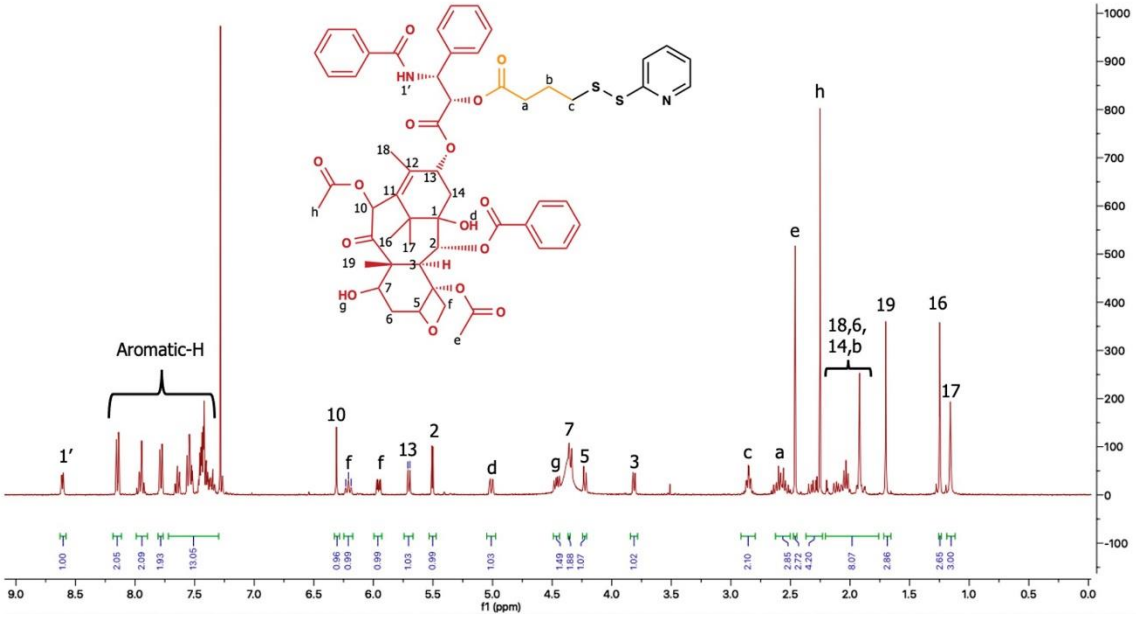

Fig. S1. ^{1}H NMR spectrum of PTX-Buss-pyr. ^{1}H NMR (400 MHz, CDCl3): δ=8.61 (d, 1H), 8.14 (m, 2H), 7.95 (m, 2H), 7.78 (m, 2H), 7.68-7.30 (m, 13H), 6.31 (s, 1H), 6.21 (t, 1H), 5.96 (dd, 1H), 5.70 (d, 1H), 5.50 (d, 1H), 5.01 (dd, 1H), 4.46 (dd, 1H), 4.37 (s, 1H), 4.22 (m, 1H), 3.81 (d, 1H), 2.85 (td, 2H), 2.59 (m, 3H), 2.46 (s, 3H), 2.37-2.22 (m, 4H), 2.22-1.75 (m, 8H), 1.66 (s, 3H), 1.25 (s, 3H), 1.16 (s, 3H) ppm.

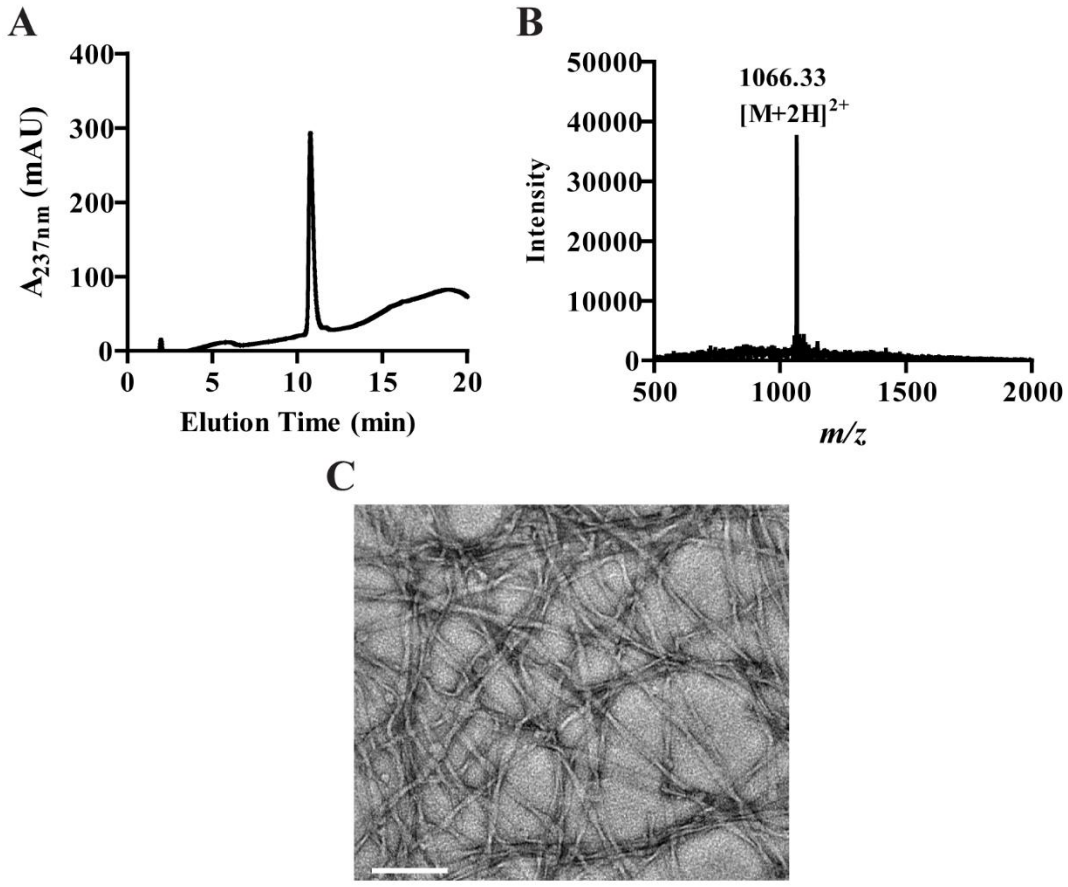

Fig. S2. Characterization of PTX-iRGD amphiphile. (A) RP-HPLC trace and (B) ESI MS profile of PTX-iRGD showing high purity and the expected molecular weight, respectively. (C) Representative TEM images of PTX-iRGD nanofilaments. Scale bar 100 nm.

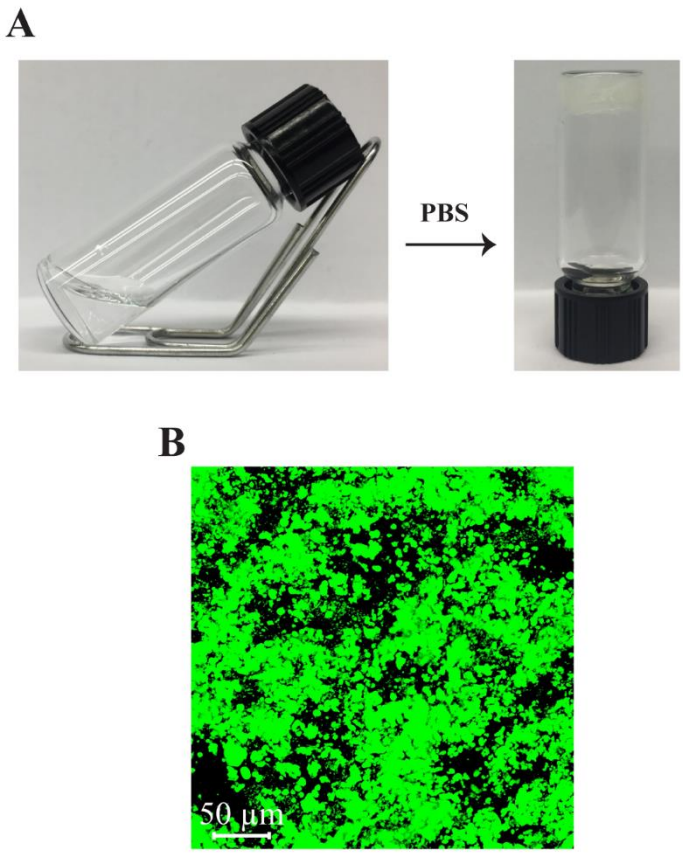

Fig. S3. Characterization of *in situ* formed aCD47/PF hydrogels. (A) Pictures of the solution-to-hydrogel transition of aCD47 loaded PF upon the addition of PBS. The hydrogel formation was not affected by the encapsulation of immunotherapeutic agents. (B) Representative CLSM image of aCD47-loaded supramolecular hydrogel, in which aCD47 was labelled with FITC. Scale bar 50 µm.

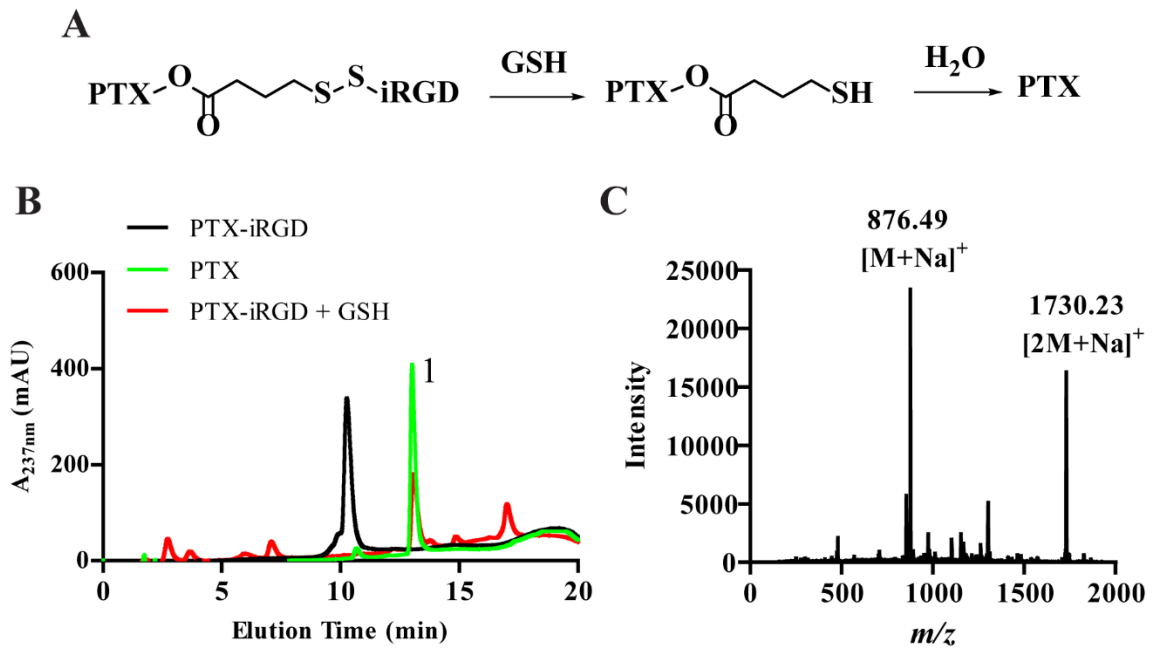

Fig. S4. Free PTX release from PTX-iRGD in the presence of GSH. (A) Mechanism of GSH induced release of PTX from PTX-iRGD. (B) HPLC profile of PTX-iRGD, PTX, and PTX-iRGD with 10 mM GSH after 8 hours at 37 ℃. (C) ESI spectra of peak 1 showing the exact molecular weight with PTX.

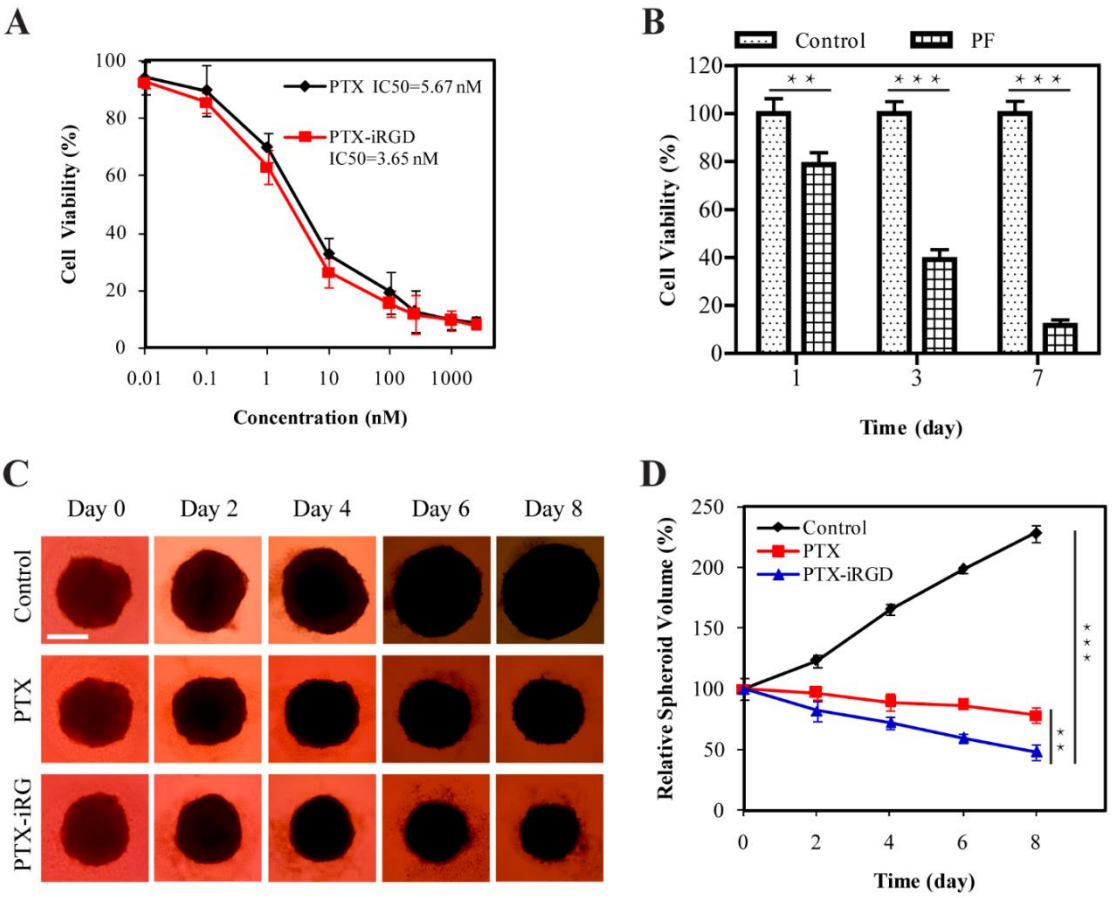

Fig. S5. *In vitro* tumor growth inhibition assay. (A) *In vitro* cytotoxicity of PTX-iRGD and (B) PF hydrogel, 3 μL of PF solution at the PTX concentration of 7.5 mM was added to each well, with DMEM as a control against GL-261 brain cancer cells. Data are given as mean ± SD (n = 3). (C) Representative images of GL-261 brain tumor spheroids on different days following treatment with free PTX or PTX-iRGD. Scale bar: 500 μm. (D) Volume of tumor spheroids treated with different formulations compared with day 0. Spheroids treated with drug-free DMEM were used as the blank control. Data are given as mean ± SD (n = 7). Statistical significance was calculated using a two-sided unpaired t-test. **P ≤ 0.01, ***P ≤ 0.001.

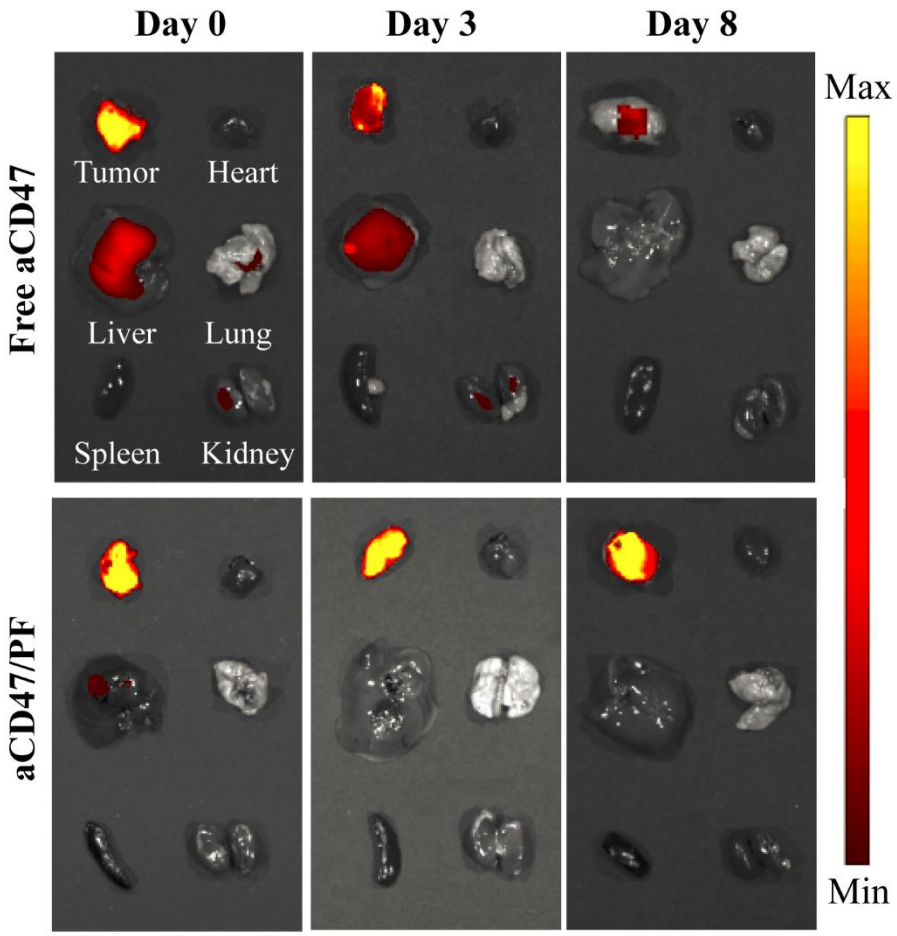

Fig. S6. Fluorescence images of major tissues from GL-261 brain tumor-bearing mice that were intratumorally injected with free aCD47 or aCD47/PF. aCD47 was labeled with Cy 5.5. Compared with free aCD47 treated mice, almost all aCD47 was trapped within the tumors of aCD47/PF injected mice, with ~62% of aCD47 remaining throughout the entire tumor after eight days.

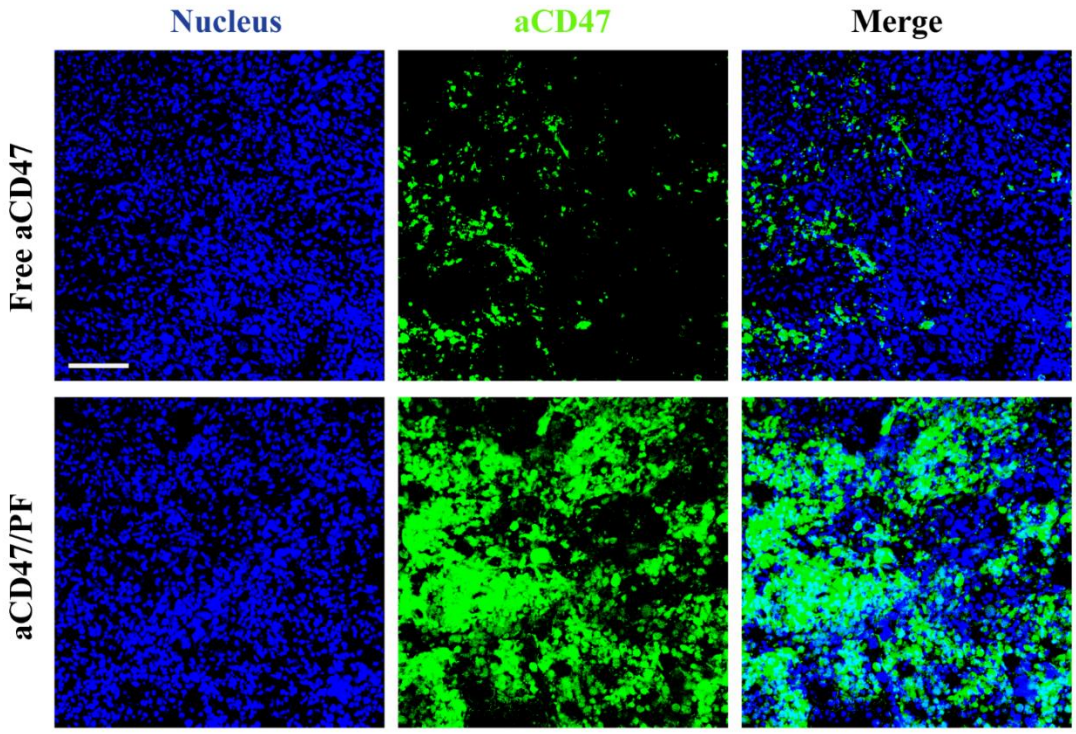

Fig. S7. Fluorescence images of tumor sections obtained three days after treatment from GL-261 brain tumor-bearing mice that were locally treated with free aCD47 or aCD47/PF. Green: FITC labeled aCD47, Blue: DAPI stained nuclei. Scale bar 200 μm. Compared with free aCD47, strong fluorescence was detected in aCD47/PF treated tumors three days following treatment.

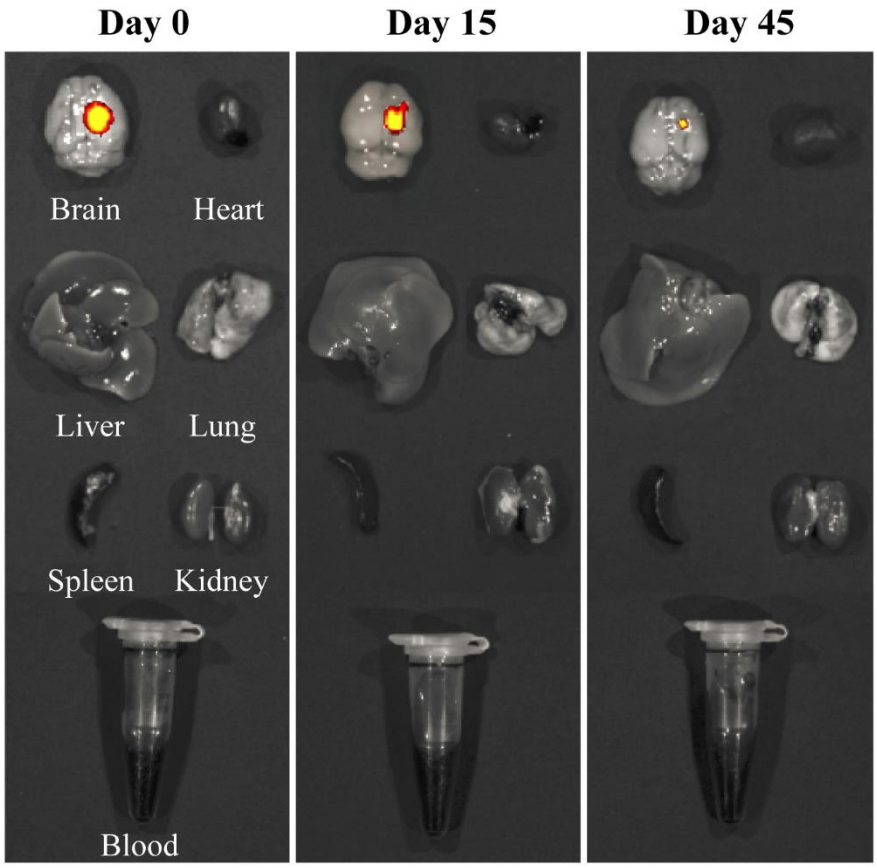

Fig. S8. Fluorescence images of major tissues from healthy mice that were intracranially implanted with aCD47/PF. Although aCD47 was gradually released from the aCD47/PF hydrogel, fluorescent signals were hardly detectable in other major organs and blood over 45 days of investigation.

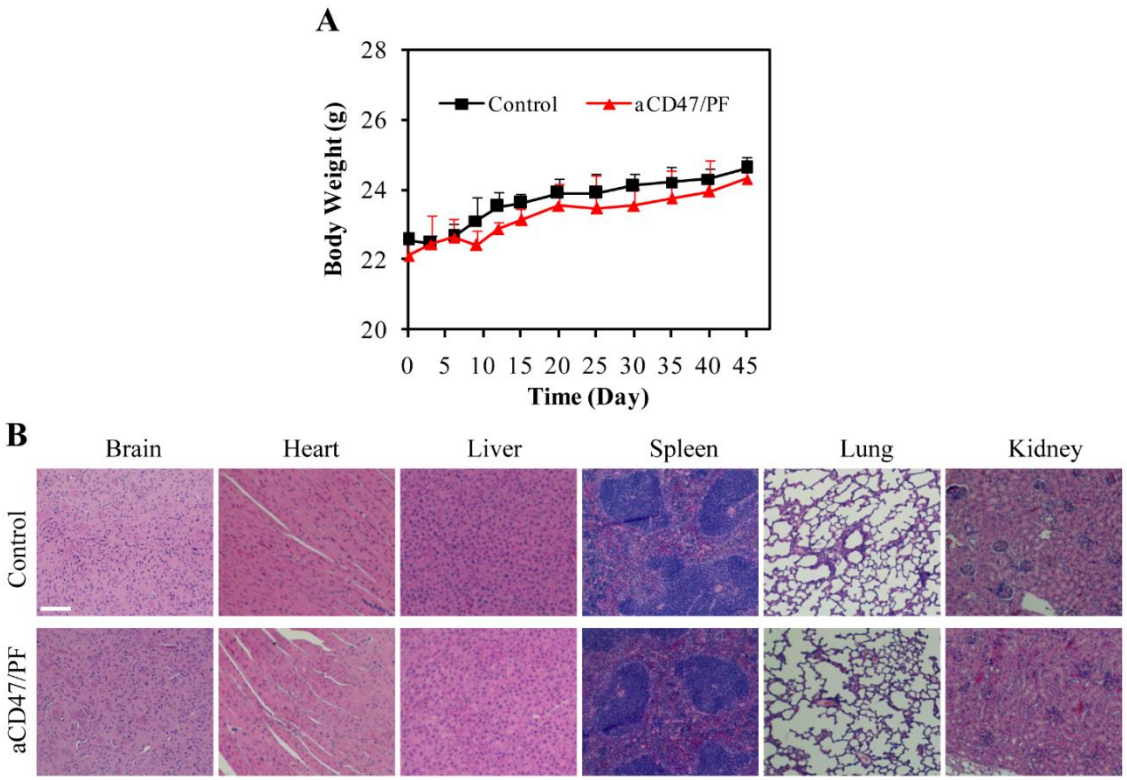

Fig. S9. Safety studies of aCD47/PF treated mice. (A) Body weight changes of mice following aCD47/PF treatment, untreated healthy mice were used as a control. Data are given as mean ± SD (n=7). No statistical difference was detected between groups. (B) H&E staining of major organs collected from healthy mice and aCD47/PF treated mice at day 45 (scale bar: 100 μm).

	RBC (M/uL)	WBC (K/uL)	PLT (K/uL)	HGB (g/dL)	HCT (%)
Reference range	7.35-11.50	3.90-13.94	545-1849	10.9-18.1	37.2-58.0
Healthy control	9.14±0.49	7.52±2.63	810±89	16.1±0.4	45.2±2.3
Day 1	9.05±0.17	9.98±1.55	754±123	16.2±0.4	44.9±1.8
Day 15	9.38±0.16	8.51±1.81	745±16	16.4±0.5	45.8±1.7
Day 45	9.23±0.19	7.62±2.18	686±11	15.9±0.1	44.1±0.8

	MCV (fL)	MCH (pg)	MCHC (g/dL)	ALP (U/L)	ALT (U/L)
Reference range	42.6-55.6	13.0-16.8	26.0-35.9	105-370	27-195
Healthy control	49.5±0.3	15.6±0.6	28.6±1.1	155±29	92±11
Day 1	46.7±1.1	15.8±0.5	29.8±1.1	200±71	104±15
Day 15	48.8±0.9	16.4±0.2	28.7±0.4	205±11	112±14
Day 45	47.8±0.2	15.3±0.3	29.3±0.5	174±10	96±11

	AST (U/L)	BUN (mg/dL)	CRE (mg/dL)	TBIL (mg/dL)
Reference range	43-397	5-26	0.2-0.5	0.2-0.6
Healthy control	85±7	21.6±2.5	0.3±0.1	0.3±0.1
Day 1	109±9	21.3±3.5	0.3±0.1	0.3±0.1
Day 15	120±28	22.5±1.7	0.4±0.1	0.4±0.1
Day 45	93±7	22.5±0.7	0.4±0.1	0.4±0.1

Fig. S10. aCD47/PF hydrogel had no significant effect on complete blood cell count and serum biochemistry. C57BL/6 mice were sacrificed on days 1, 15, and 45 after aCD47/PF treatment. Untreated healthy mice were used as a control. Complete blood cell counts data including: RBC, WBC, PLT, HGB, HCT, MCV, MCH, and MCHC. Serum biochemistry data including: ALP, ALT, AST, BUN, CRE, and TBIL. Data are presented as mean ± SD (n=3). Reference ranges of hematology data of healthy C57BL/6 mice were obtained from Charles River Laboratories.

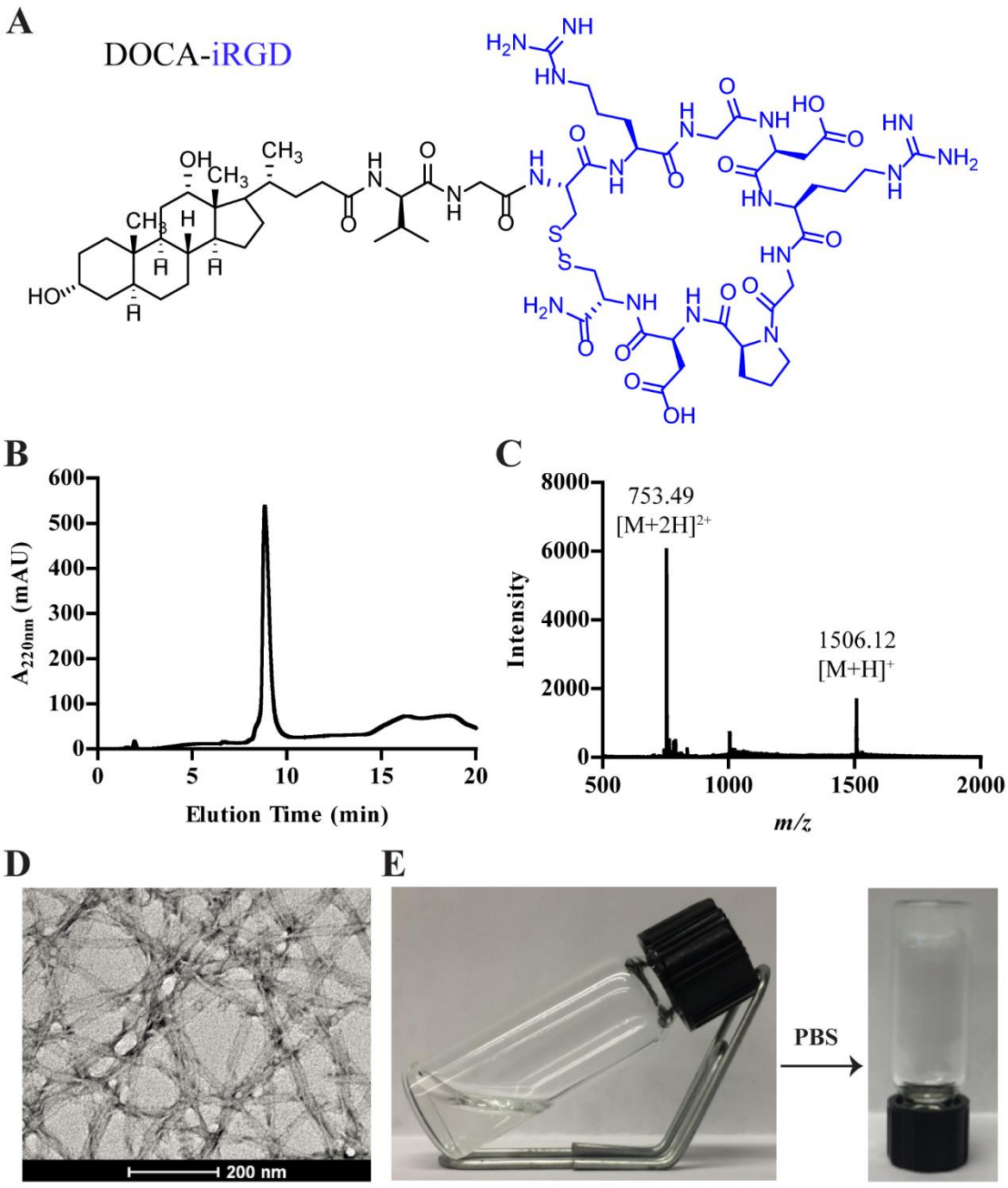

Fig. S11. Characterization of the designed DOCA-iRGD as an *in situ* formed, drug-free hydrogel. (A) Chemical structure of the DOCA-iRGD amphiphile. (B) RP-HPLC trace and (C) ESI MS profile of the DOCA-iRGD conjugate showing high purity and the expected molecular weight, respectively. (D) Representative TEM images of DOCA-iRGD filamentous nanostructures. Scale bar 200 nm. (E) Pictures of the solution to hydrogel transition of DOCA-iRGD filamentous nanostructures with the addition of PBS.

Treatment	Number	Median survival	Long-rank test
Blank	8	28.5	
EF	8	29.5	ns *vs*. Blank
PF	8	63	*** *vs*. Blank
aCD47/EF	8	39	** *vs*. EF
aCD47/PF	8	Undefined	*** *vs*. Blank

Fig. S12. Median survival for animals treated with different therapies. Statistical significance was determined using a two-sided unpaired t-test. ***P ≤ 0.001. The combined aCD47/PF treatment resulted in an extraordinary benefit in median survival.

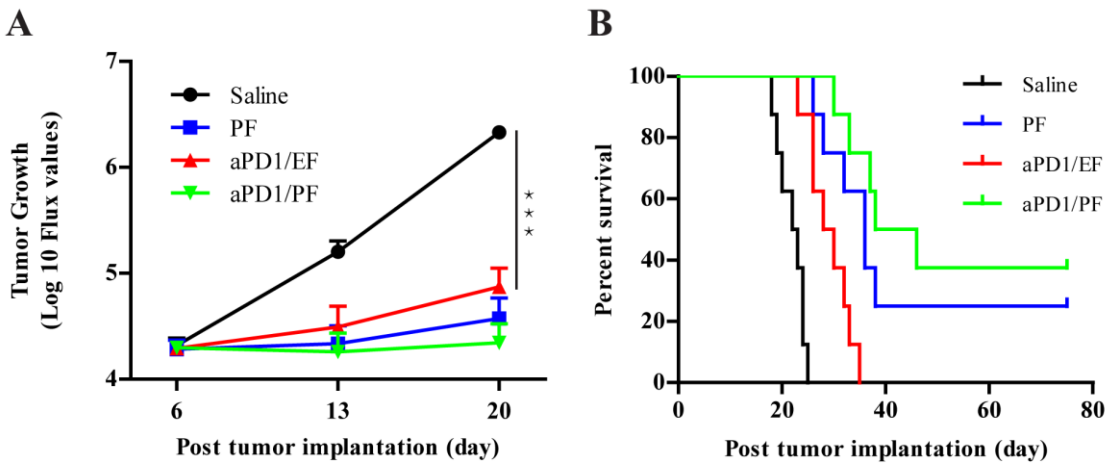

C

Treatment	Number	Median survival	Long-rank test
Blank	8	22	
PF	8	36	*** *vs.* Blank
aPD1/EF	8	29	** *vs.* aPD1/PF
aPD1/PF	8	42	ns *vs.* PF

Fig. S13. Anti-cancer efficacy of the aPD1/PF hydrogel on mice bearing GL-261 brain tumor. aPD1/PF was prepared in the same procedure as aCD47/PF. aPD1/PF was directly injected into established brain tumors on day 6 post-tumor implantation. The dosages of administered drugs were 50 μg of aPD1 and 150 μg of PTX per mouse. (A) Quantification of tumor growth from bioluminescence imaging of the GL-261 tumors in the indicated treatment groups. (B) Survival curves corresponding to indicated treatment groups. Statistical significance was calculated via the log-rank (Mantel-Cox) test. (C) Median survival for brain tumor bearing mice treated with different therapies. There is no significant difference between aPD1/PF (Green) and PF (Blue). Statistical significance was determined using a two-sided unpaired t-test. Data are given as mean ± SD (n = 3). **P ≤ 0.01, ***P ≤ 0.001.

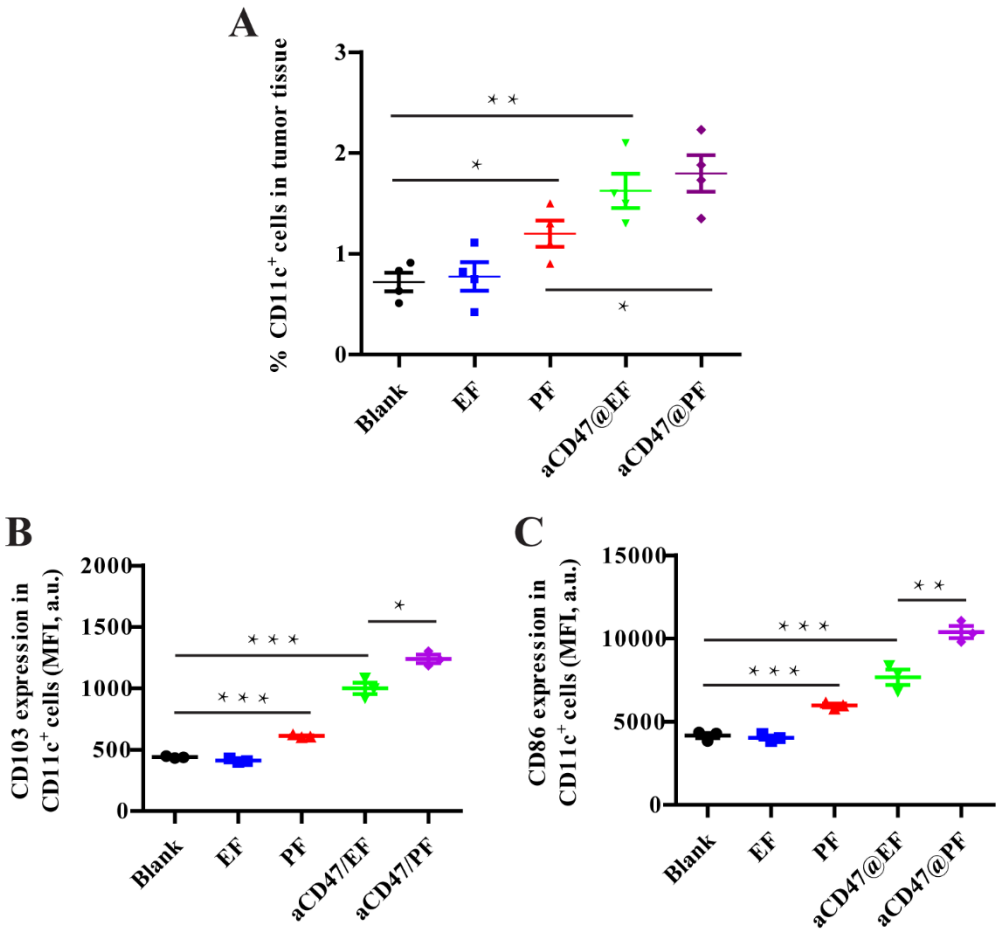

Fig. S14. aCD47/PF hydrogel induced infiltration of dendritic cells in tumor tissues. (A) The absolute percentage of $CD11c^+$ cells in the tumor tissue. (B) Quantification of $CD103^+$ and (C) $CD86^+$ dendritic cells in the indicated treatment groups. Statistical significance was determined using a two-sided unpaired t-test. Data are given as mean ± SD (n = 3). *P ≤ 0.05, **P ≤ 0.01, ***P ≤ 0.001.

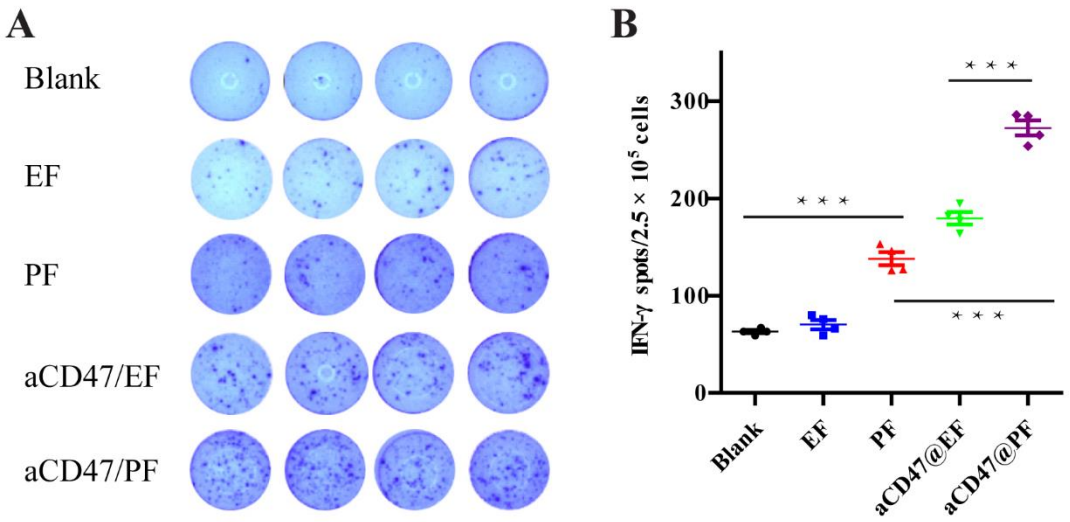

Fig. S15. aCD47/PF treatment induced robust antigen-specific T-cell immune responses. (A) Representative images of an ELISpot assay and (B) statistical data from restimulated PBMCs determined by the ELISpot assay on day 7 post different treatment. Statistical significance was determined using a two-sided unpaired t-test. Data are given as mean ± SD (n = 4). ***P ≤ 0.001.

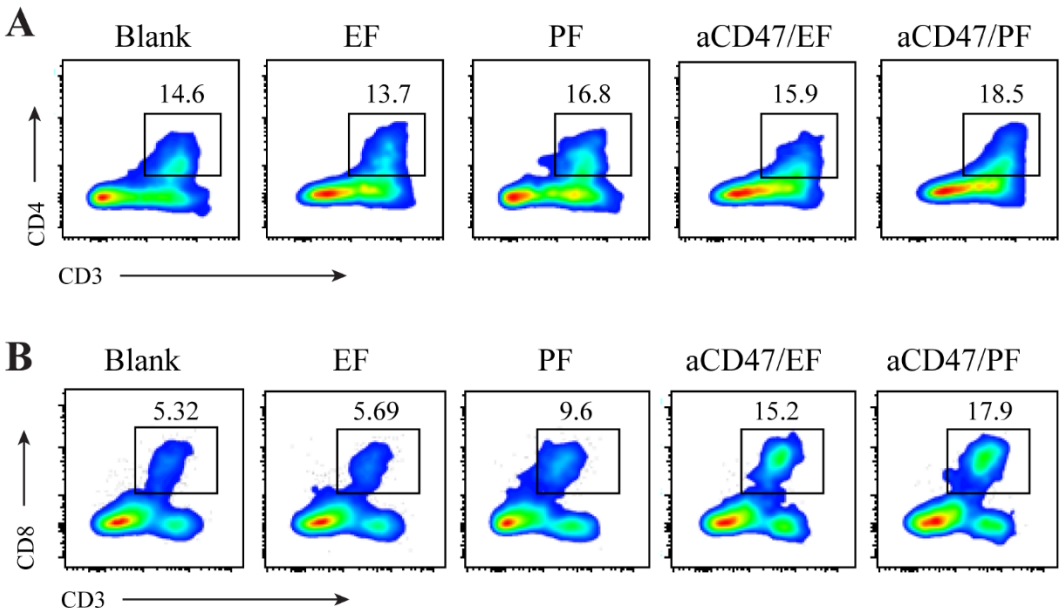

Fig. S16. aCD47/PF hydrogel induced infiltration of T cells in tumor tissues. (A) Representative flow cytometric analysis of $CD4^+$ T cells and (B) $CD8^+$ T cells within tumors in different treatment groups.

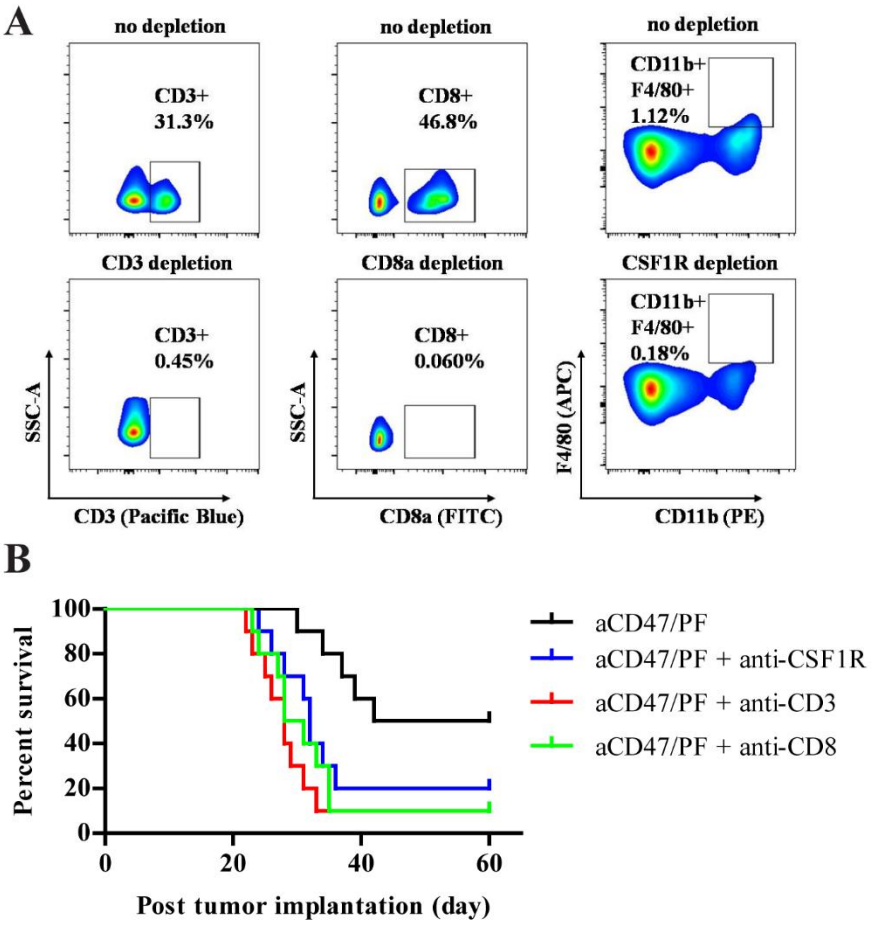

Fig. S17. CD3⁺ T cells, CD8⁺ T cells and macrophages are critical to the observed aCD47/PF induced tumor growth inhibition. (A) Depletions of CD3⁺ T cells, CD8⁺ T cells and macrophages were confirmed using flow cytometric analysis of PBMCs after aCD47/PF and appropriate antibody treatment. (B) Survival curves of GL-261 brain tumor-bearing mice treated after with aCD47/PF along with CD3⁺ T cells, CD8⁺ T cells and macrophages depletion. (n = 10 for each group). Statistical significance was calculated via the log-rank (Mantel-Cox) test. *P ≤ 0.05, **P ≤ 0.01.

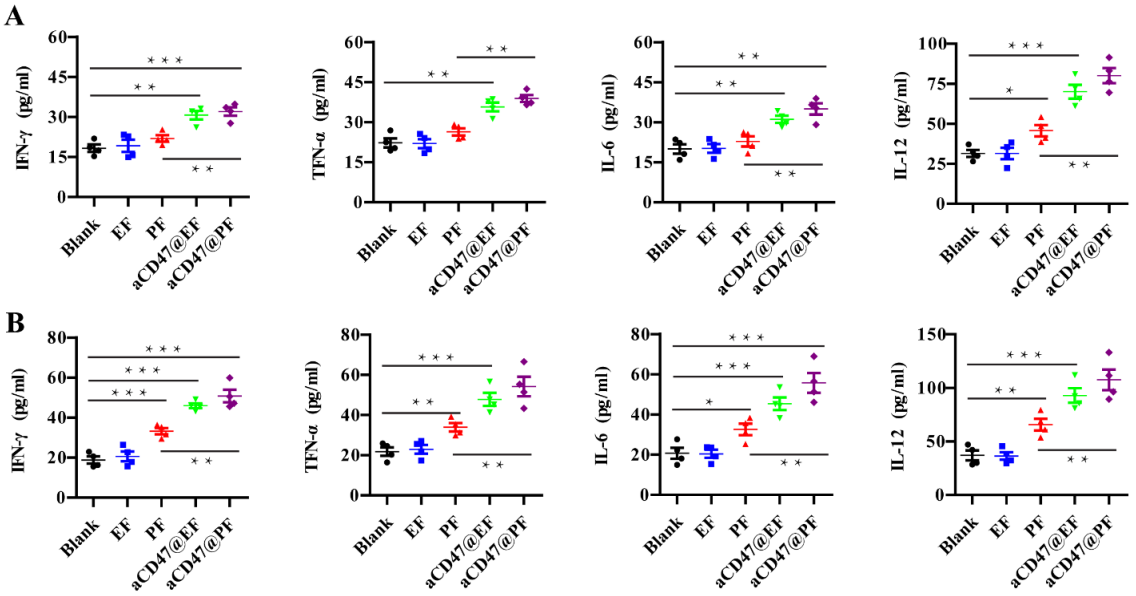

Fig. S18. aCD47/PF treatment elicited increased secretion of IFN-γ, TNF-α, IL-6, and IL-12. (A) Secretion levels of IFN-γ, TNF-α, IL-6 and IL-12 at day 1 and (B) day 3 post different treatments. Statistical significance was calculated using a two-sided unpaired t-test. Data are given as mean ± SD. *P ≤ 0.05, **P ≤ 0.01, ***P ≤ 0.001.

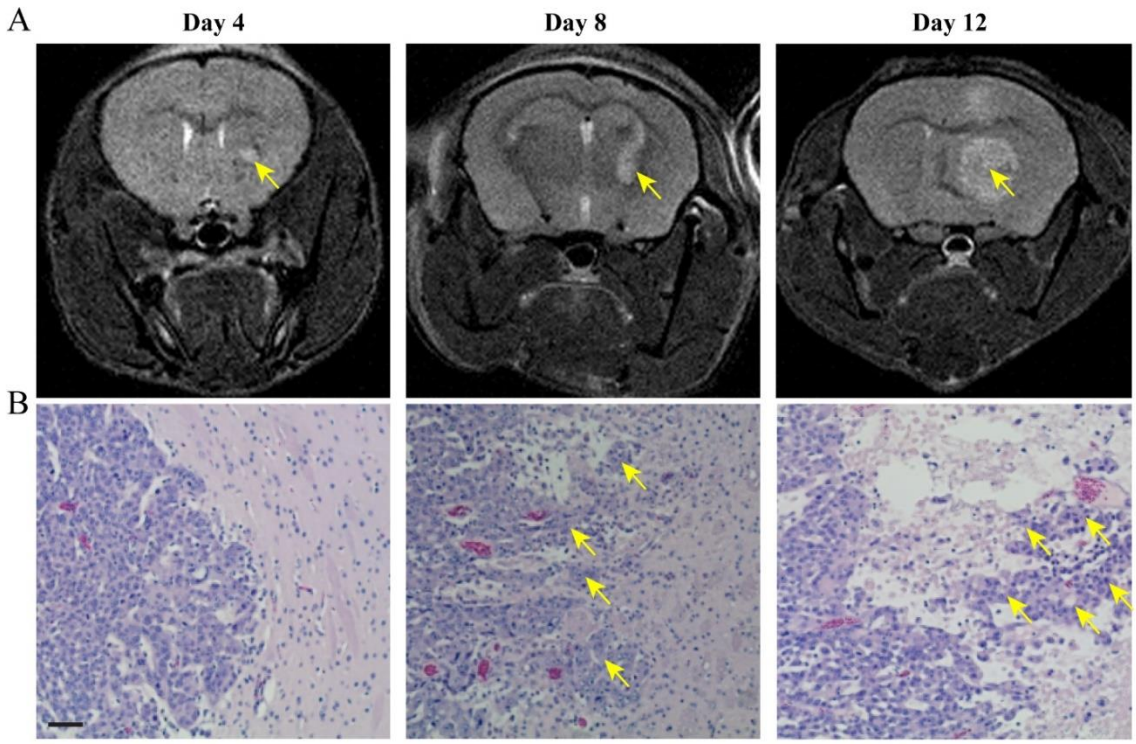

Fig. S19. MRI imaging and H&E staining to determine the optimal day for brain tumor resection. (A) T2 weighted MR images of GL-261 brain tumors monitoring tumor growth at day 4, 8, and 12 post implantation. Lighter zones indicated by yellow arrows show tumor location within the brain. (B) H&E staining of the brain sections that display tumor growth at day 4, 8, and 12 post implantation. Yellow arrows indicate invading tumor cells or islands of tumor cells around the primary tumor mass. Scale bar, 100 μm. GL-261 brain tumors had developed 4 days after inoculation, but these tumors were inadequate in size and no tumor cell invasion was observed, therefore all tumor tissue could be completely removed. Beyond day 12, the exponential development of tumors resulted in overgrowth and several big islands of tumor cells observed around the primary tumor mass and inside the surrounding normal brain parenchyma. Consequently, the tumor mass could not be excised adequately, leaving the majority of tumor intact following resection. At day 8 post-implantation, the tumor was proper in size with small tumor deposits around the primary tumor mass. From this data, we ascertained that the optimal day for surgical resection was day 8 post-inoculation.

A

Treatment	Number	Median survival	Long-rank test
Blank	8	28.5	
EF	8	29.5	ns *vs.* Blank
PF	8	63	*** *vs.* Blank
aCD47/EF	8	39	** *vs.* EF
aCD47/PF	8	Undefined	*** *vs.* Blank

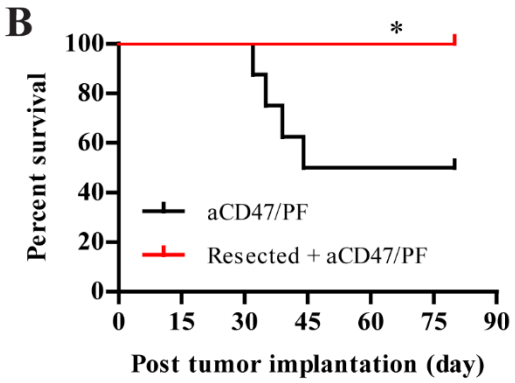

Fig. S20. aCD47/PF hydrogel inhibited brain tumor recurrence after resection. (A) Median survival for brain tumor resected mice treated with different therapies. Statistical significance was determined using a two-sided unpaired t-test. (B) Survival curves for non-resected and resected mice treated with aCD47/PF. Statistical significance was determined via the log-rank (Mantel-Cox) test. *P ≤ 0.05, **P ≤ 0.01, ***P ≤ 0.001.

SI References

1. M. A. Navarrete, C. Bertinetti-Lapatki, I. Michelfelder, H. Veelken, Usage of standardized antigen-presenting cells improves ELISpot performance for complex protein antigens. *J. Immunol. Methods* 397, 146-153 (2013).
2. Moller, K. Michel, N. Frech, M. Burger, D. Pfeifer, P. Frommolt, H. Veelken, A-K. Thomas-Kaskel, Dendritic cell maturation with poly(I:C)-based versus PGE2-based cytokine combinations results in differential functional characteristics relevant to clinical application. *J. Immunother.* 31, 506-519 (2008).
3. K. D. Moynihan, C. F. Opel, G. L. Szeto, A. Tzeng, E. F. Zhu, J. M. Engreiyz, R. T. Williams, K. Rakhra, Eradication of large established tumors in mice by combination immunotherapy that engages innate and adaptive immune responses. *Nat. Med.* 22, 1402-1410 (2016).